

Seismic imaging of the Hussar low frequency seismic data

A.Nassir Saeed, Gary F. Margrave, David C. Henley, J. Helen Isaac and Laurence R. Lines

ABSTRACT

We have implemented an effective seismic processing flow that meets both AVO compliant and seismic imaging objectives for the Hussar low frequency seismic data. The ground roll and pump-jack noise that poses great challenge in seismic processing and imaging of the Hussar low frequency experiments were successfully attenuated and removed via cascaded radial trace filters, while retaining reflection energy of low frequency down to 3Hz.

The resulting migrated section from the new processing shows significant imaging improvement across the entire section, and particularly in the shallow zone (100-500m) that was not clearly seen in previous processing. The zoomed pre-stack migrated sections show more stratigraphic phenomena, such as onlap and pinch-out features that were not clearly shown in the post- stack migrated section. The phase coherency of the estimated band signal show good spatial coherency down to 3Hz in the processed stacked section.

The resulting common image gathers, (CIGs) have shown good reflectivity signal at the far offset of 3450m (an increment of 57%) compared to the 1980m far offset produced by contracting processing company.

INTRODUCTION

In 2011, CREWES collaborated with Husky Energy, INOVA and GeoKinetics to acquire seismic data using different source (dynamite and VibroSeis) and geophones types (10Hz 3C and 4.5Hz geophones and VectorSeis accelerometers) with the aim of recording very low frequency seismic data down to 2Hz (Margrave et al., 2012).

The survey site is located at Hussar, Alberta, and with hydrocarbon targets within the Glauconitic sand channel and Ellerslie formations. According to the literature these two prospects are respectively gas and oil charged formations. Figure (1) shows the location of survey line, which is 4.5 km long where several wells owned by Husky energy intersect survey lines.

The Hussar seismic datasets have been processed by CREWES (Isaac and Margrave, 2011; Henley, 2012) as well as by a contracted processing company. Figure (2) shows two common image gathers (CIGs) from the pre-stack Kirchhoff migration. Note that the residual noise left its signature as a step ladder pattern in the CIG gather which complicates the interpretation of the seismic section, and questions the noise attenuation techniques used. Furthermore, note also that a maximum offset bin of 1980m in the CIG gather will probably affect the accuracy of inverted elastic attributes from the pre-stack (AVO) seismic inversion.



FIG.1. The location of the 4.5 km seismic survey line for the Hussar low frequency experiments.

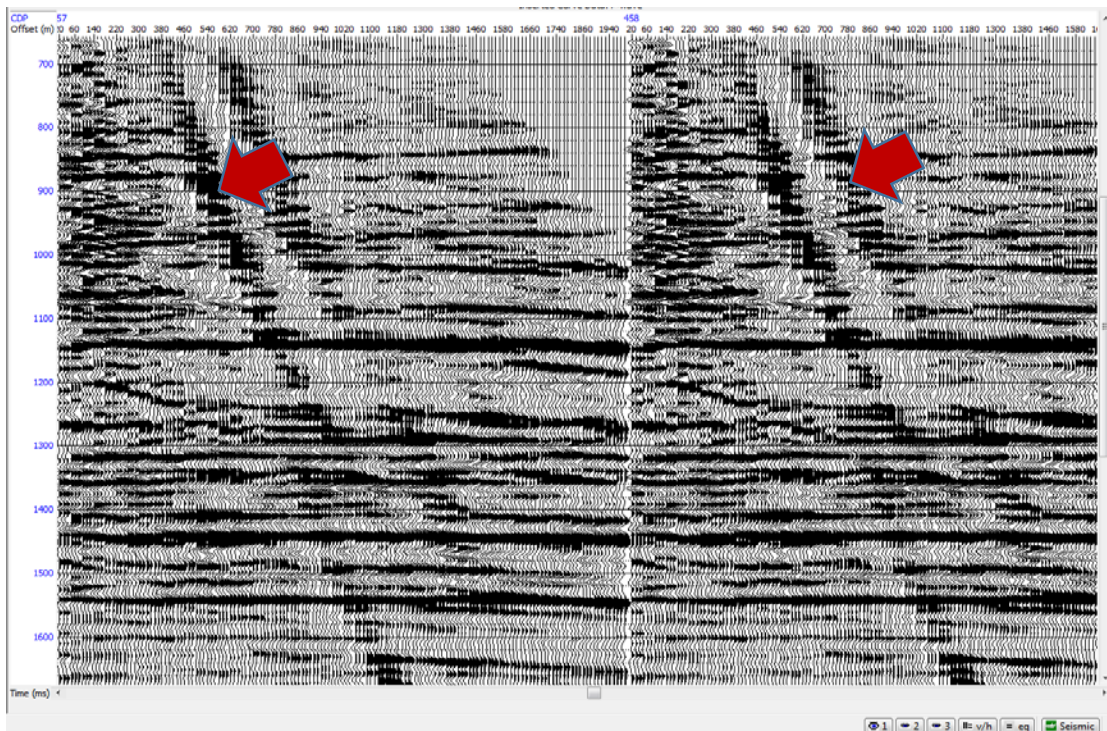


FIG.2. Common image gather, CIG, from a processing contractor. Note the residual noise signature as a step-ladder pattern (indicated by arrows) left in the CIG gathers. Also note the maximum far offset of 1980 m.

Hence, in this report, we have designed a seismic data processing flow applied to different seismic data sets acquired during the Hussar low frequency experiments. The objectives are to preserve very low frequency signal down to 3Hz in the seismic reflectors while attenuating different types of seismic noise, improve seismic imaging sections, and push the far offset bin in the CIG gathers to maximum feasible distances where reflectivity signals in the zones of interests can be fairly mapped.

In the following section, we highlights steps used in seismic data processing and noise attenuation techniques. This is followed by comparison made from resulting seismic sections from post stack and pre-stack migration. Bandwidth estimation of seismic signals is also presented.

SEISMIC DATA PROCESSING OF THE HUSSAR SEISMIC DATA

The seismic data processing flow given in Table (1) is aimed to be AVO compliant, and has been applied to three different seismic datasets of the Hussar P-wave data (the dynamite and vibroSeis seismic sources using 10Hz geophones as well as VectorSeis accelerometers). In this report, we will present results of seismic data processing for the seismic dataset that was acquired using a dynamite source with conventional 10Hz geophones only.

Table 1. Processing flow for the Hussar low frequency seismic data

Processing flow: Hussar 2D line
Reformat & Geometry assignment
Trace and shot edit
Amplitude recovery
Apply datum and refraction statics
Noise suppression: Radial filter , air blast
Surface Consistent Gabor Deconvolution
Two passes of velocity analysis Surface Consistent Residual Statics
PSTM gathers preparation
Pre Stack Time Migration
Post migration Gabor Deconvolution
FX noise attenuation
Mute & Stack

Seismic noise, such as, ground-roll and pump-jack noise (see Figure 3) predominantly affect raw gathers, and poses great challenges in attenuating noise while preserving reflection signal at very low frequencies. Since such noise has specific velocity and dip characteristics at specific frequency band levels, radial trace filtering (Henley, 1999) is a robust method to attack and attenuate this noises. Figure 4, shows the results after applying radial filters, where the apparent velocity of these dipping noise events at 1-2.5Hz are analyzed and were successfully attenuated. Note that the shot gather in Figure 4 shows better continuity of reflection energy at the middle of the gather (around 1200-1800ms), as well as reflection signal at shallow time that were masked by refraction and ground-roll noise. Furthermore, the gather after applying radial filtering shows consistent energy distribution across the gather, as much energy due to ground-roll and pump-jack noise has been attenuated.

Note that although we attempted to make the seismic processing flow meet the principles of AVO compliant processing, we did not apply surface-consistent amplitude correction before deconvolution, as it produced null values for deconvolved gathers. This null problem is beyond the scope of this report, and is being investigated. Fortunately the raw gathers after applying amplitude recovery followed by radial filtering showed consistent amplitude and energy distribution across the gathers.

Surface-consistent Gabor deconvolution (Margrave et al., 2002) has been applied since our objective is to use CIG gathers as input for AVO inversion of the Hussar low frequency seismic data. The windowed-Fourier Gabor deconvolution is a nonstationary minimum-phase spike deconvolution method, designed to estimate and remove both source signature and subsequent earth attenuation effects (Margrave et al., 2004). Thus, it provides better reflectivity continuity for deep reflectors compared to conventional surface-consistent deconvolution algorithm (Levin, 1989).

Figure 5 shows a shot gather before deconvolution. The estimated inverse deconvolution operator is refined, and then subsequently applied, resulting not only in broadening the amplitude spectrum of the raw gathers, but also attenuating residual low frequency noise (Figure 6) was left after applying radial filtering to seismic noise whose frequency bandwidth were above the assigned frequency band $> 2.5\text{Hz}$ in the radial filtering. Note the broad spectrum of a shot gather. Note that some low frequency noise manifests in the centre of the deconvolved gather in Figure 6 has frequency band $>3\text{-}16\text{ Hz}$, and can be attenuated if the noise train is modeled first and then subtracted from the gather (Saeed, 2013). However, we decided to leave them as their frequency bandwidths are within frequency bandwidth of some reflectors, and these noises will be attenuated when the seismic data are stacked.

All seismic datasets went through two cycles of velocity analysis followed by surface-consistent residual static corrections except the Vibroseis data, which required three cycles of velocity analysis and residual static corrections. Figure 7 shows the structure stack section of the dynamite 10Hz after the second pass of residual static corrections. The stacked section shows excellent mapping and continuity of reflectors from very shallow events all the way to the end of the sections.

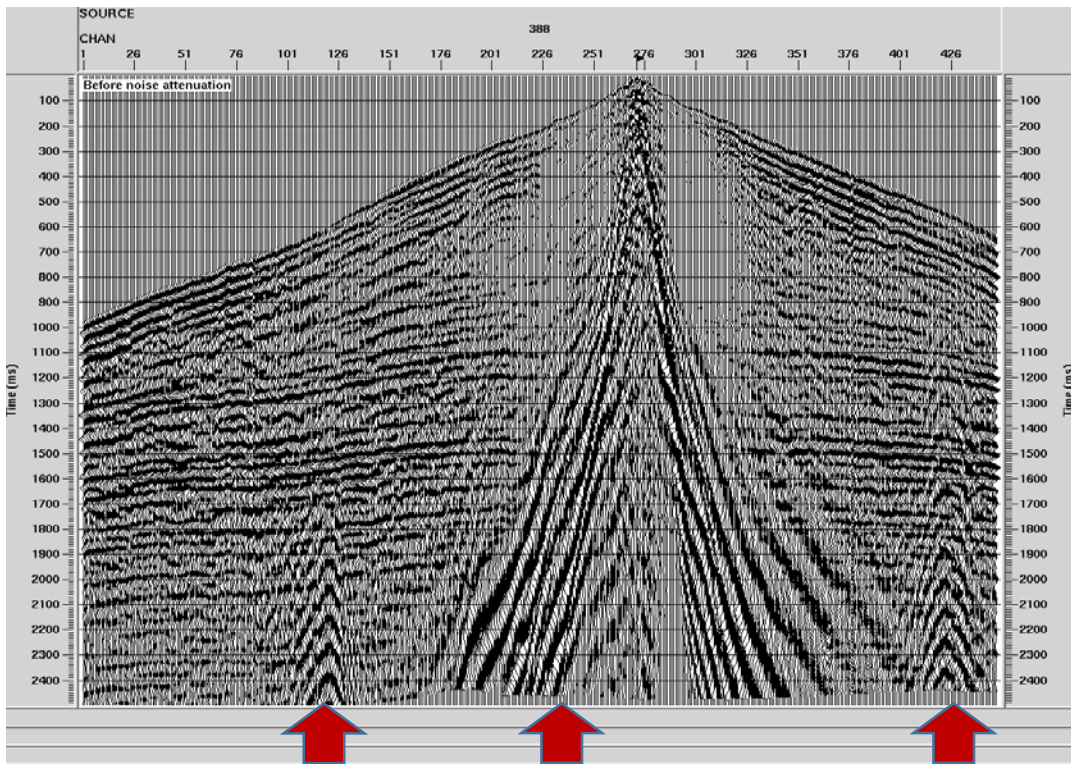


FIG.3. Shot gather before noise attenuation via radial filtering. The arrow in the middle refers to ground-roll noise while side arrows refer to pump-jack noise.

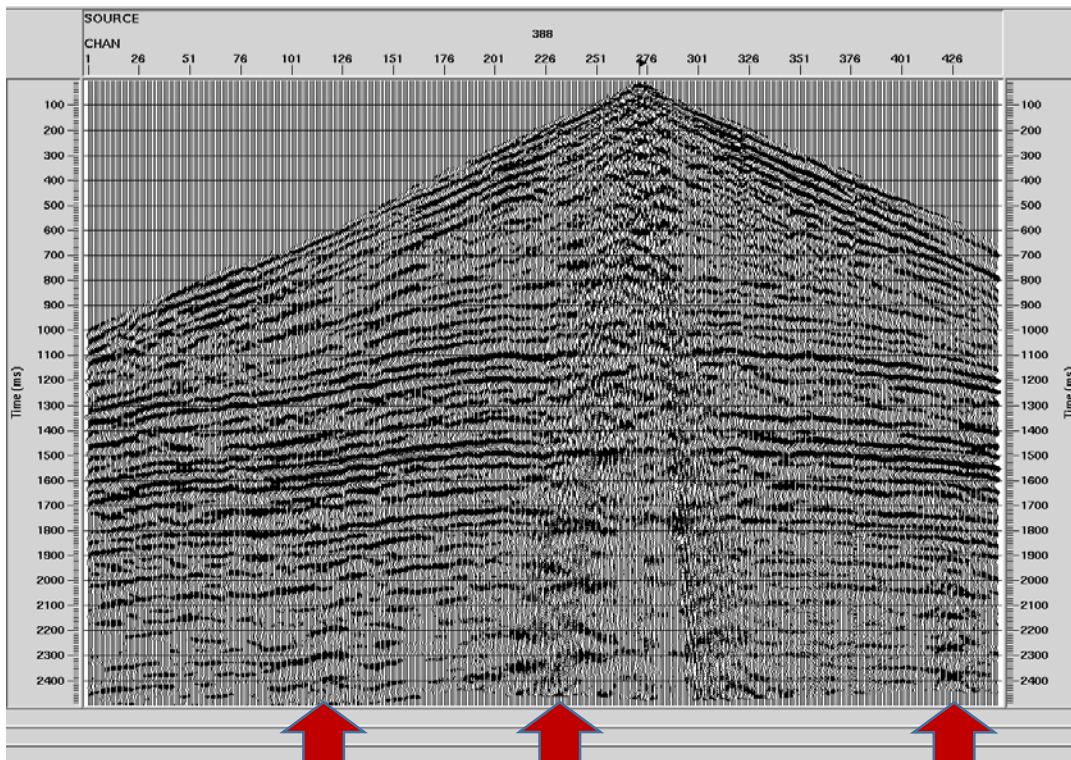


FIG.4. Shot gather after applying noise attenuation via radial filtering.

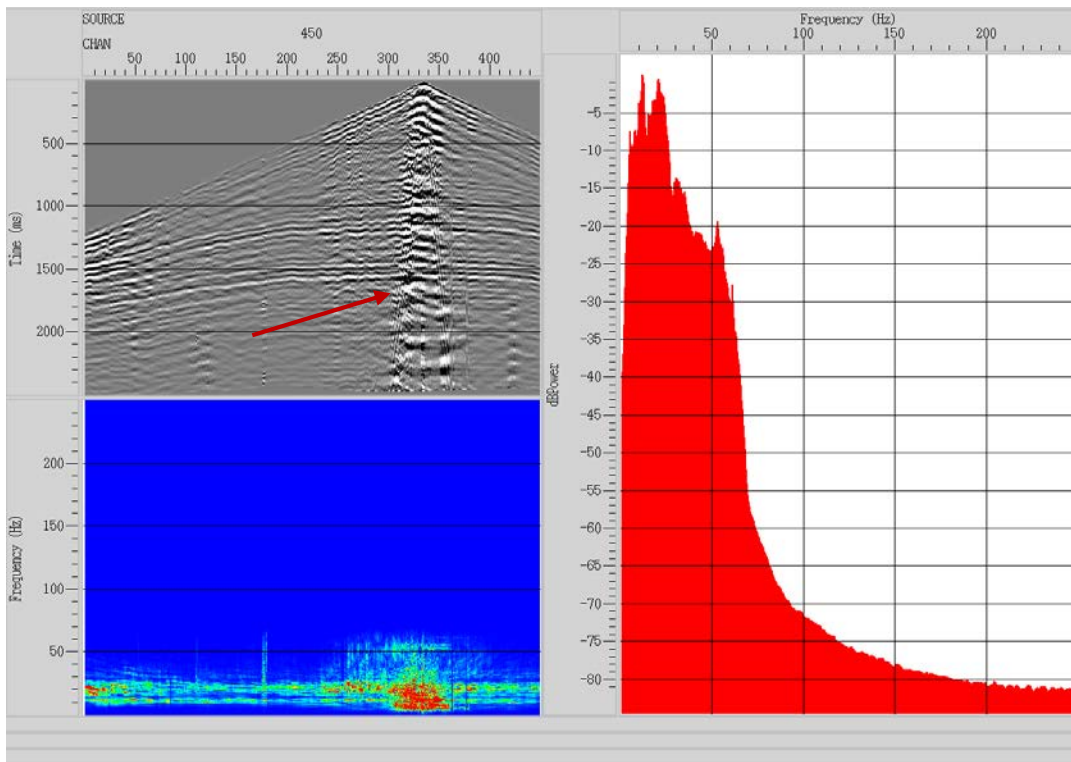


FIG.5. Shot gather before applying surface-consistent Gabor deconvolution.

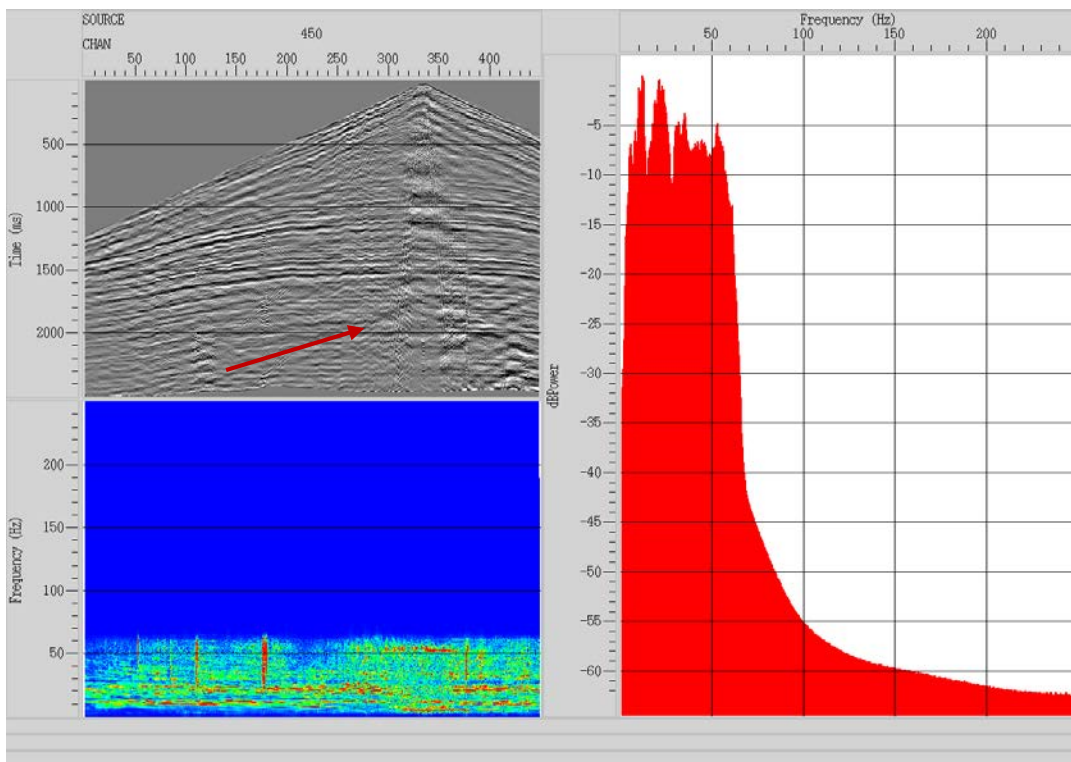


FIG.6. Shot gather after applying surface-consistent Gabor deconvolution. Note the low frequency noise close to the arrow location is further attenuated.

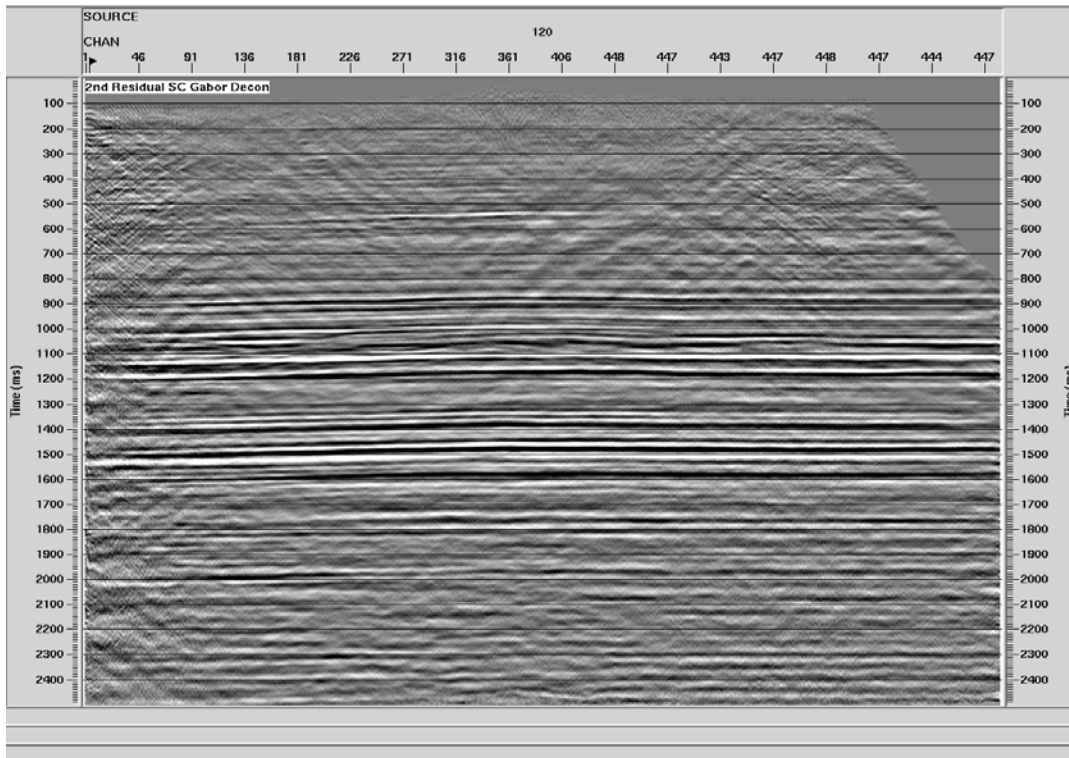


FIG.7. Structure stack section after second pass of residual statics applied for the Hussar dynamite source recorded with 10Hz geophones.

SEISMIC IMAGING OF THE HUSSAR LOW FREQUENCY DATA

We have performed post-stack and pre-stack migration for the Hussar low frequency data using Kirchhoff and phase-shift migration algorithms. For post stack migration, we noticed the resulted migrated section using the Kirchhoff algorithm did not reveal much reflection information for the shallow events (100-500 ms) compared to the phase-shift migration algorithm. Hence, we will only show stacks of phase-shift post migrated section in this report.

Figure 8a shows a post-stack phase-shift migrated section, while Figure 8b shows the same stacked section but with post migration Gabor deconvolution applied. Note the overall improvement in frequency bandwidth content of the post migrated Gabor section; most noticeably the high resolution reflectivity events in the shallow part of the stack section where more detailed reflectors at 100-500ms are manifested.

Pre-stack migration preparation includes offset binning to ensure uniform distribution for all offset bins of the shot gathers used in the pre-stack migration. For pre-stack imaging, tests were conducted for optimal apertures distances, maximum dip, stretch mute and maximum offsets used to constrain the common image gathers resulting from pre-stack migration. Furthermore, residual migration velocity analyses were also conducted to adjust velocity percentages in spatial and temporal directions of the sections.

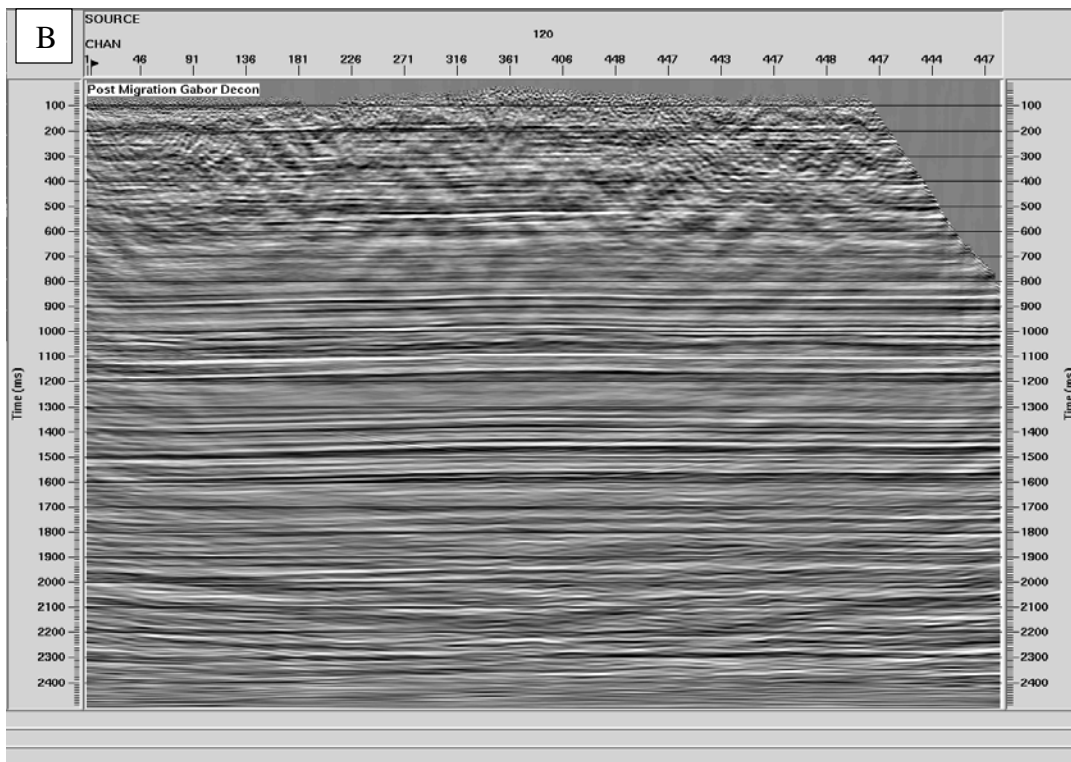
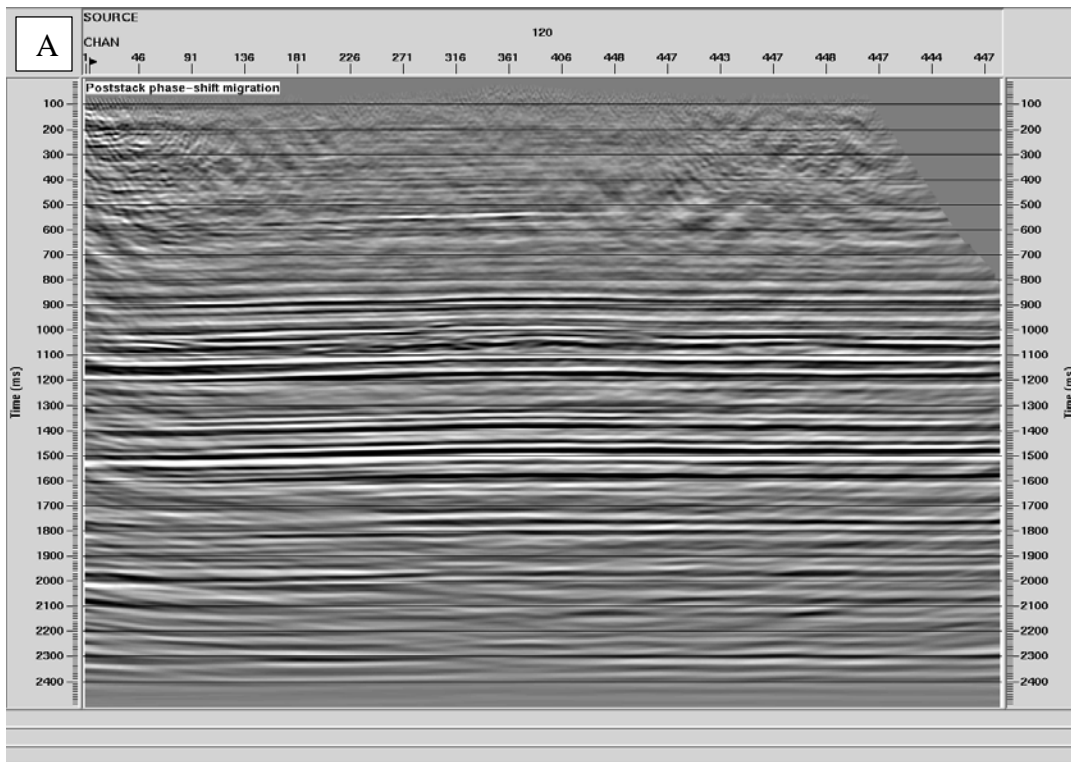


FIG.8. Poststack phase-shift migration section. (A) Before applying post migration Gabor deconvolution. (B) After applying post migration Gabor deconvolution.

Figure 9 shows the migration velocity for the dynamite 10Hz geophone data after smoothing. The common image gather in Figure 10 shows good seismic imaging and correct assigned velocity values for different reflectors. The frequency content and resolution of the common image gathers are further enhanced by applying post migration Gabor deconvolution followed by FX-deconvolution to clean up some random noise expected from pre-stack imaging.

In terms of AVO perspective, applying post migration Gabor deconvolution should still preserve AVO signature in the common image gathers, as a wider windowed-Fourier sliding window was used. Furthermore, since a global operator across the CIG gather is applied, the amplitude variation with offset will still be preserved. However, the frequency content will be changed. Of course the final say on the impact of applying post migration Gabor deconvolution can be made by comparing synthetic offset gather with the extracted seismic offset gather close to a well.

Figure 11a shows the section from our Pre-stack Kirchhoff migration, while Figure 11b shows the same section from processing company. Note that the contractor has chosen a different datum elevation, replacement velocity, output bin offset and post migration zero phase deconvolution. Therefore, we cannot make bench mark comparison for each reflector, as a bulk shift is needed to tie same events in both stack sections. Hence, the comparison is made based on overall seismic imaging and resolution. The pre-stack image section of data processed by us shows superior resolutions for events from 500-900ms. Furthermore, the contractor's section show some undulating features, particularly at CDP 351 and CDP 651, that affect the reflectivity of events above and below the zones of interests (900-1200ms). These anticline-shaped features do not represent a marked geological structure in the survey area and are probably due to overestimated velocity values and statics at these specific locations, as the section processed by us shows expected flat events above and below the Glauconitic and Errelslie formations (~1050-1150 ms). However, the processing company's section shows better seismic imaging at the left side of the low fold area.

Figure 12 shows sections of both post-stack and pre-stack phase-shift migration processed for this report. Both show excellent stacked sections, and more details and better seismic resolutions are achieved in the pre-stack phase shift migration compared to the post-stack phase-shift migration.

Figures 13-15 show respectively, decimated zoomed sections of post-stack phase-shift migration, pre-stack phase-shift migration and pre-stack Kirchhoff migration. The following comparison notes are observed:

Post- and Pre- stack Phase-shift migration: the zoomed post stack section (Figure 13) shows clean and strong reflectivity amplitudes compared to the pre-stack migrated section (Figure 14). However, more channel-like shapes (at time 1020-1120ms) as well as onlap and pinch-out features are evident at CDP 575 and CDP 725 respectively.

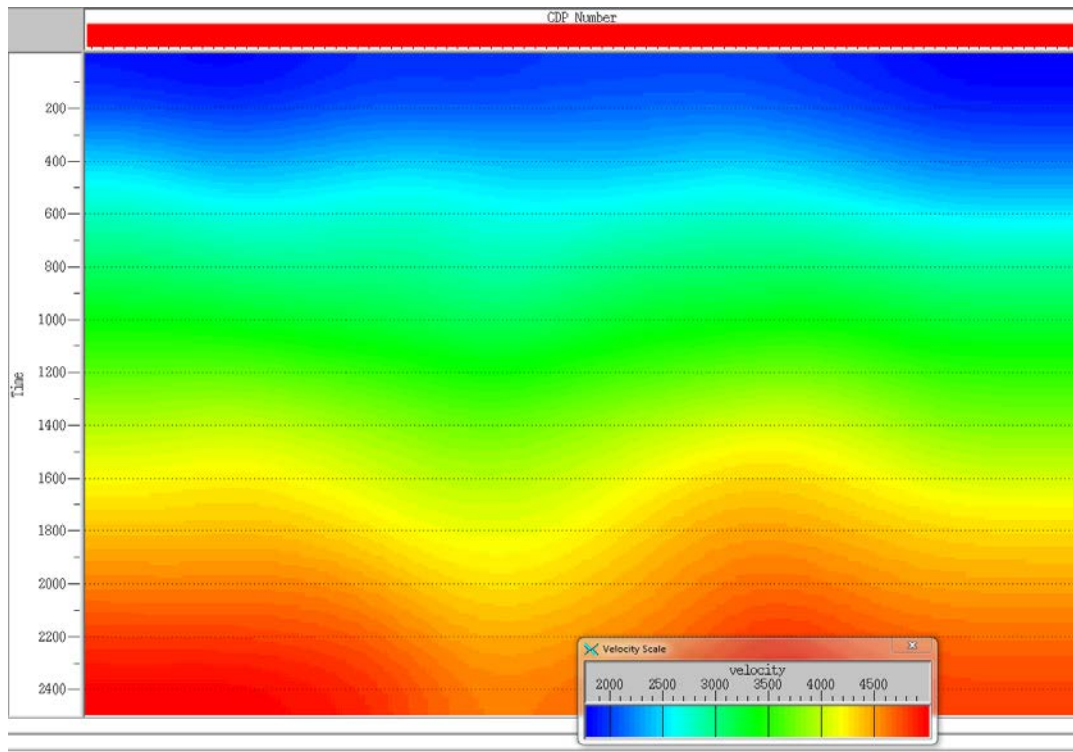


FIG.9. Migration velocity section for the Hussar dynamite data recorded with 10 Hz geophones.

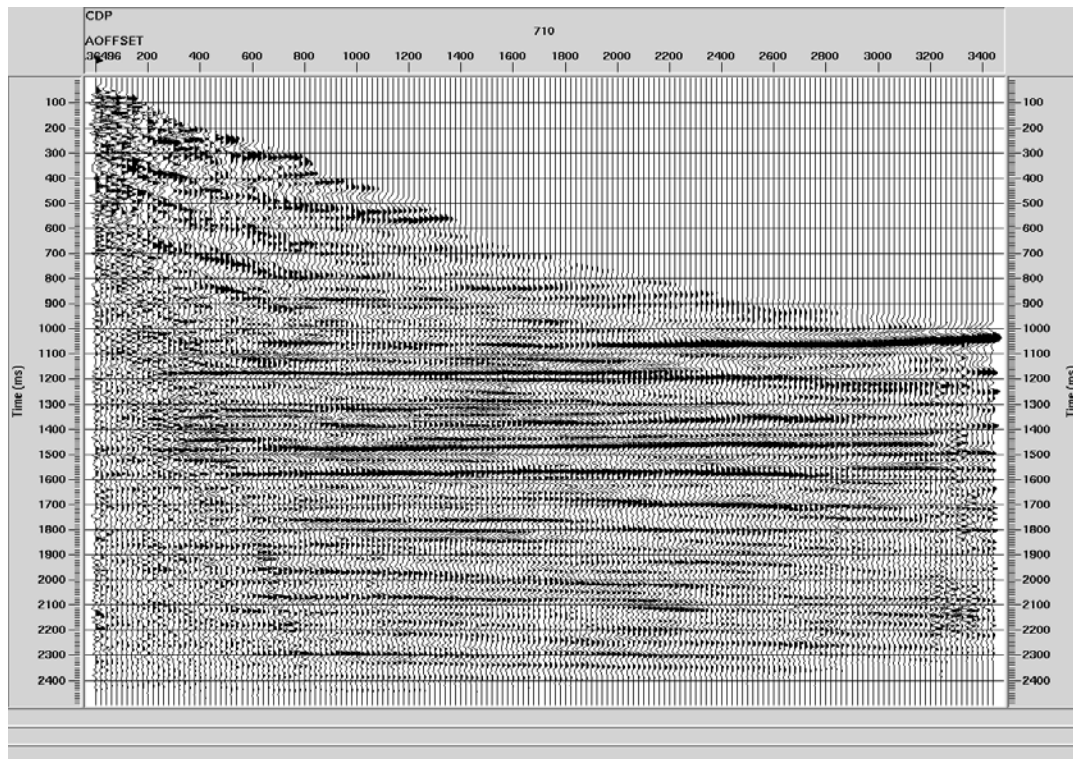


FIG.10. Common image gather, CIG, from pre-stack Kirchhoff migration.

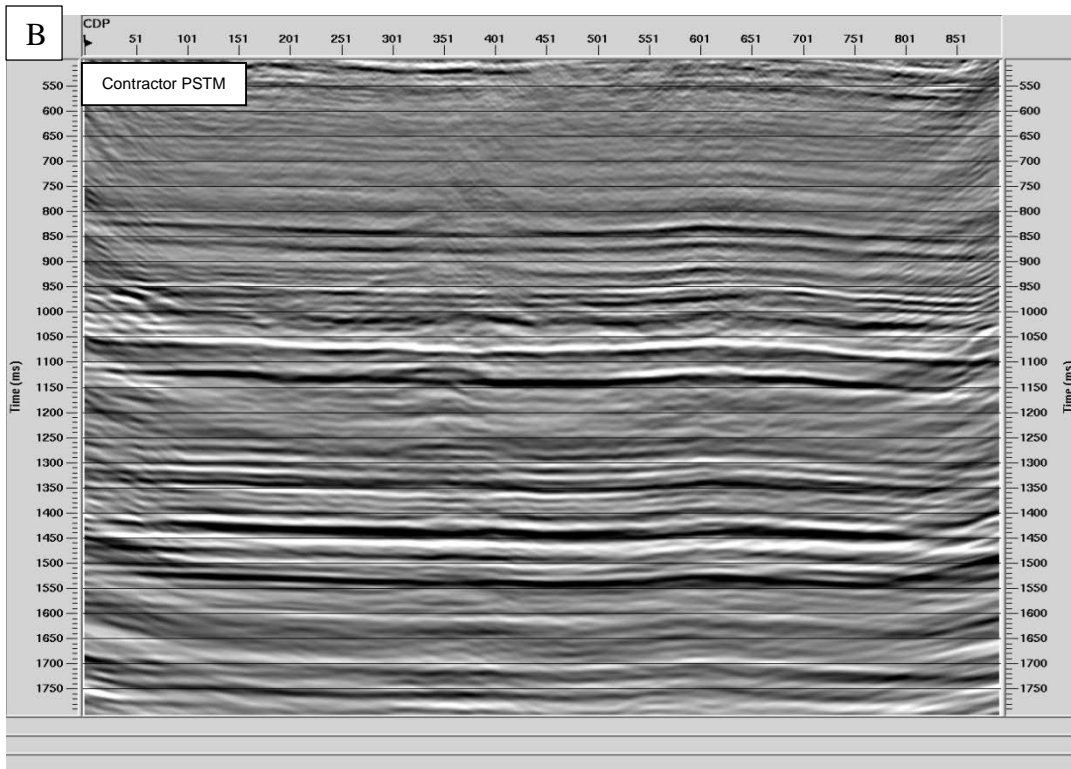
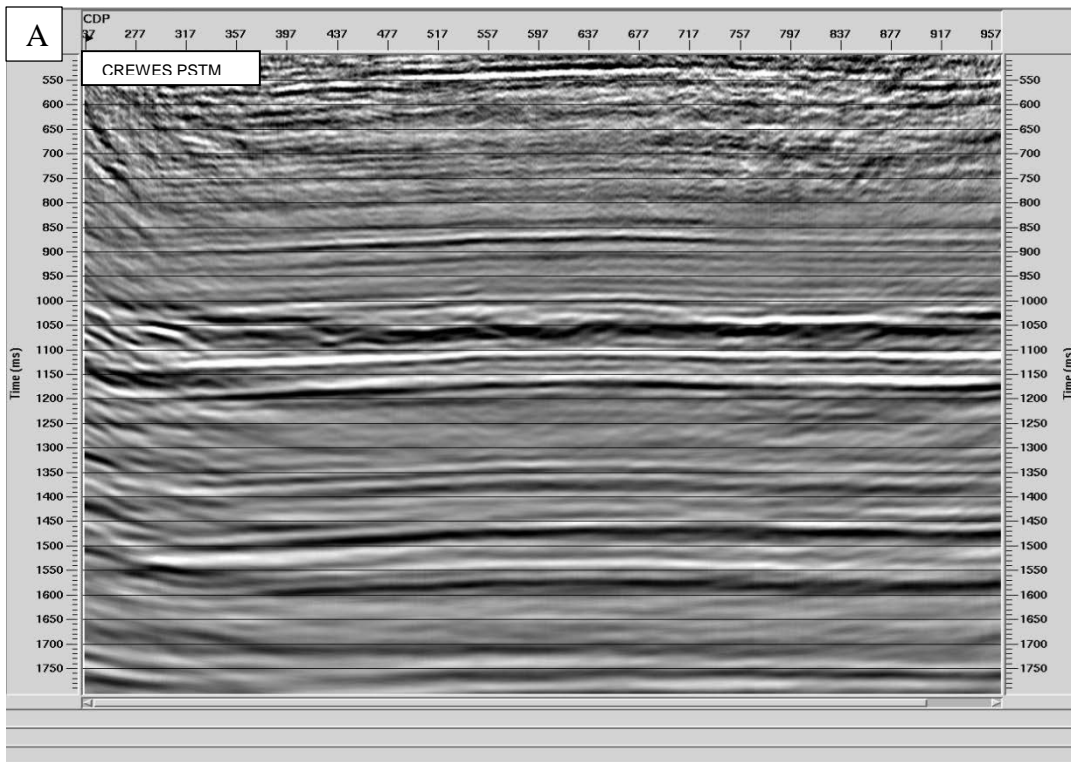


FIG.11. Pre-stack Kirchhoff migrated section. (A) Processed in this report. (B) Processed by contracting geophysical processing company.

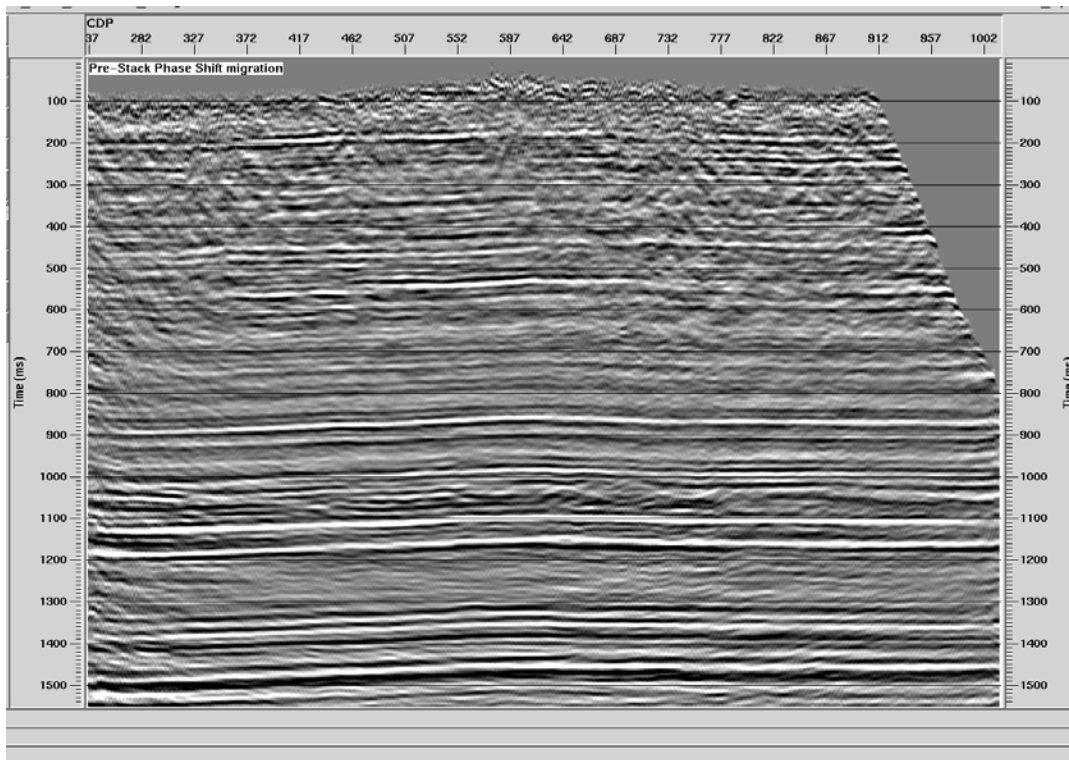
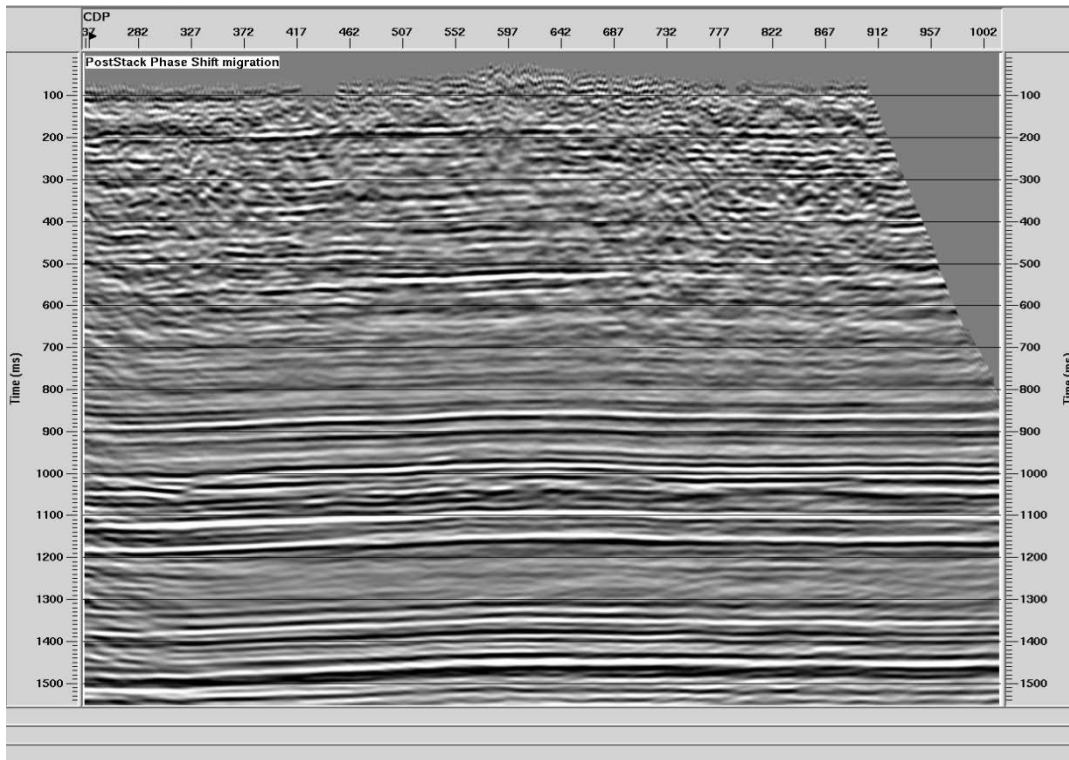


FIG.12. Top: Post-stack phase-shift migration section. Bottom: Pre-stack phase-shift migration section. Note that better resolution and continuity are achieved in pre-stack phase-shift migration section.

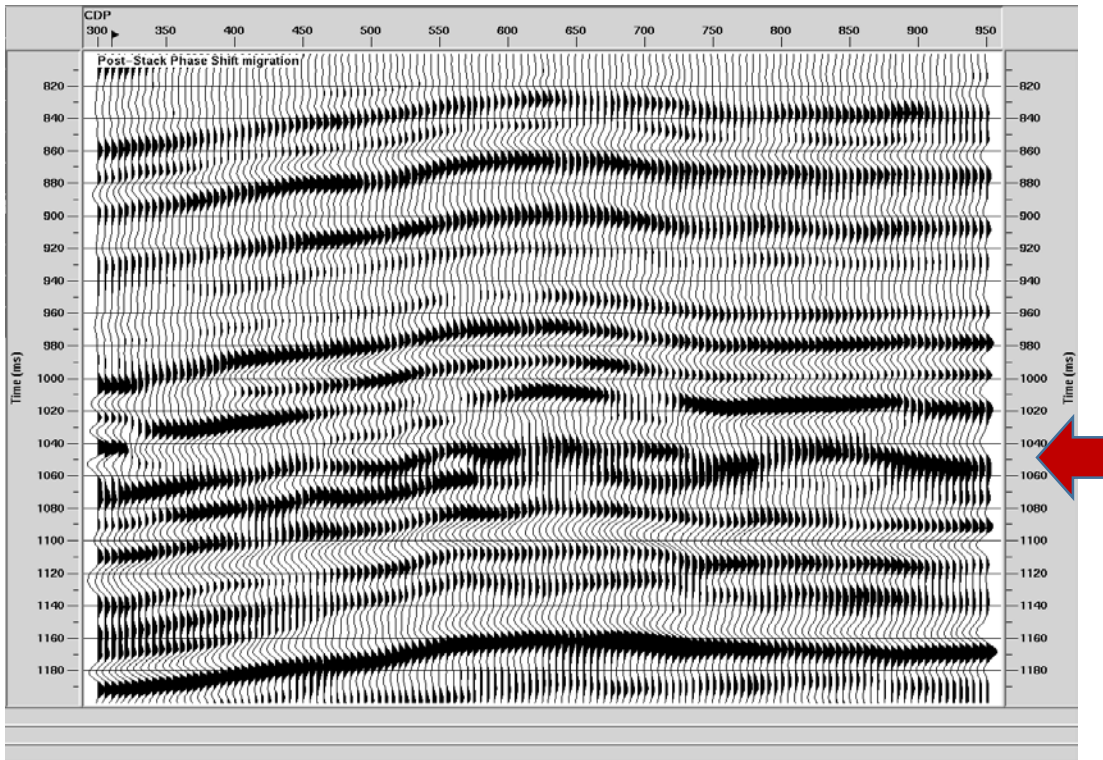


FIG.13. Zoomed section from decimated stack of post-stack phase-shift migration. Zone of interest is from 1020-1120ms.

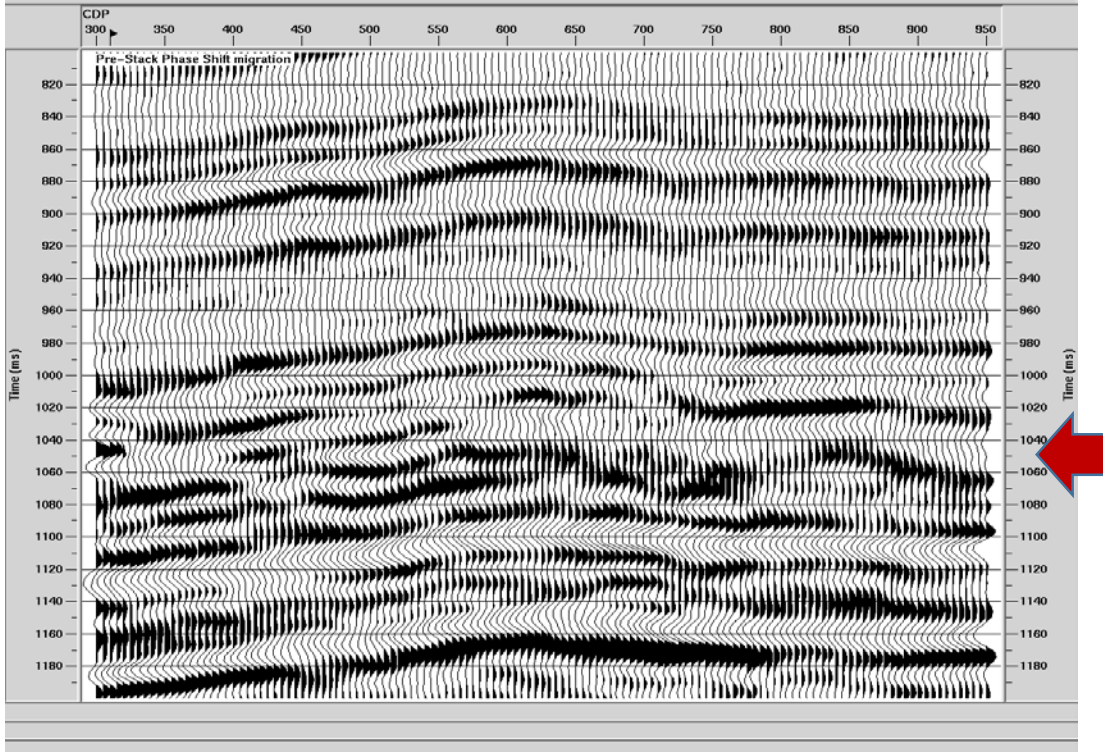


FIG.14. Zoomed section from decimated stack of pre-stack phase-shift migration. Zone of interest is from 1020-1120ms.

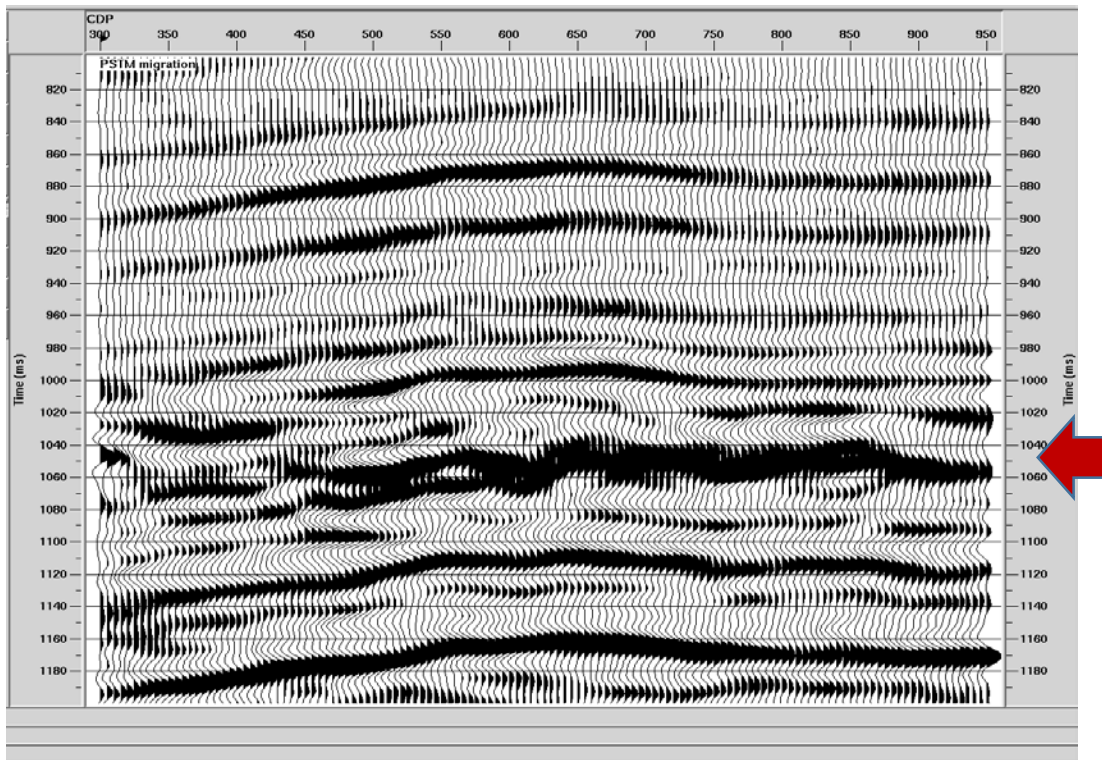


FIG.15. Zoomed section from decimated stack of pre-stack Kirchhoff migration. Zone of interest is from 1020-1120ms.

Pre-stack Kirchhoff and Phase-shift migration: The Pre-stack phase-shift migration (Figure 14) reveals more stratigraphic depositional features, as indicated above compared to the Pre-stack Kirchhoff migrated section (Figure 15). However, reflectors showing strong continuity are better mapped in the Pre-stack Kirchhoff section. One possibility for the difference in signatures in the zone of interest (1020-1120ms) in both stack section is that the Kirchhoff algorithm is probably applying the proper migration phase rotations for 3D while the phase-shift is inherently 2D. In theory, this causes a 45 degree phase rotation (Bleisteinet al., 2001).

SEISMIC SIGNALS BAND ESTIMATION

The estimation of the seismic bandwidth of the stacked section (Margrave, 1999) gives an indication about efficiency of the applied processing flow in retaining reflectivity signal while removing unwanted ground-roll noise and other low frequency signals in the desired time window and frequency band limit. The aim of the Hussar seismic experiment is to record low frequencies. Isaac et al, (2013) analysed the low frequency content of the seismic data acquired at Hussar.

Figure 16 shows measured phase-coherency, which shows spatial coherence of seismic signal for the processed dynamite with 4.5Hz geophone as well as phase-coherency of 4.5Hz geophone (VectorSeis) dataset processed by Henley (2012). The processed stacked section (Figure 16a) shows strong phase coherence signal down to 5Hz, and in many areas along the section it shows good coherence down to 2Hz. However, the coherence of Vectorseis section (Figure 16b) shows strong coherence at 7Hz, and good coherence down to 4Hz in areas not affected by noise.

On the hand, the measured amplitude-coherency of both sections given in Figure 17 shows strong amplitude coherence down to 7Hz, particularly for the VectorSeis stack (Figure 17b) processed by Henley (2012) compared to the dynamite 4.5Hz geophones section (Figure 17a) processed by us. However, the 4.5 Hz stacked section shows strong amplitude spatial coherence across entire section compared to the Vectorseis stacked section of Henley (2012) that shows fair amplitude spatial coherence.

CONCLUSION

The pre-stack image sections produced from the seismic processing flow applied in this study show superiority in terms of seismic resolution and reflectivity continuity at very shallow part compared to the pre-stack image sections from a seismic processing contractor. Furthermore, we were able to extend the far offset in the CIG gather to 3450m, an increment 57% from the 1980 m far offset of the processing contractor, and resulting common image gathers are free from the step-ladder shape of residual noise that were evident at the CIG gathers produced by the processing contractor. The processed seismic data preserved reflectivity down to 3Hz. Noise attenuation via radial filtering was able to successfully attenuate ground-roll and other seismic noise, while maintain reflectivity at very low frequencies.

We also show improvements in both phase- and amplitude- spatial coherence in the processed stack section down to 2Hz. The estimated signal band attributes indicate the robustness of the processing flow in preserving very low frequency of the reflector signal and removing unwanted ground-roll and other low frequency noise.

ACKNOWLEDGEMENTS

We thank the CREWES sponsors for financial support of this study. We also thank Husky Energy, GeoKinetics, INOVA, ION-Sensor and CREWES staff, and students for their contributions to the Hussar low frequency experiments. We also appreciate the contribution of Landmark processing software.

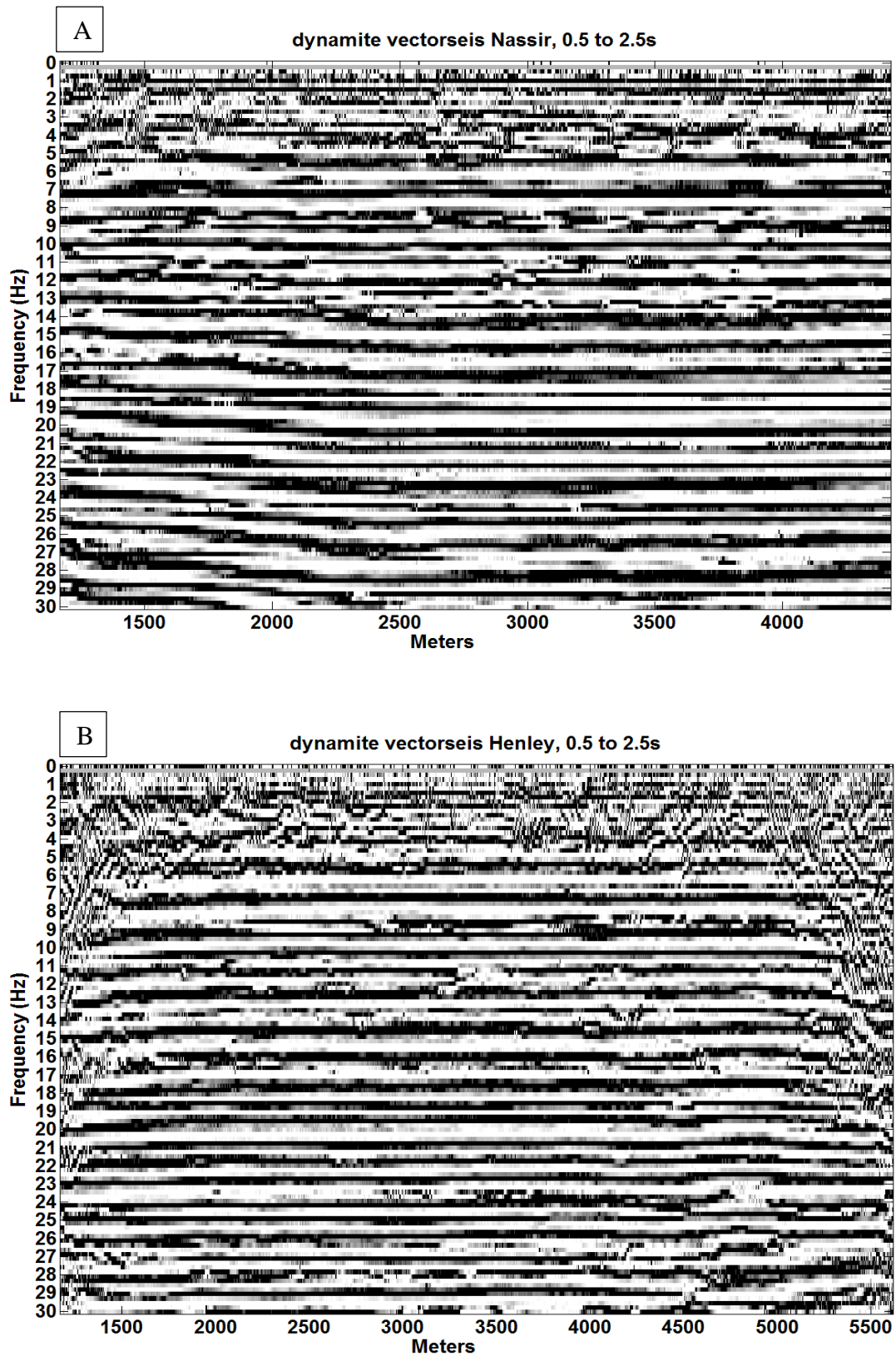


FIG.16. (A): Phase coherency plot for stack section for the dynamite with VectorSeis accelerometers. (B): Phase coherency plot for stack section for the dynamite with VectorSeis accelerometers (Henley, 2012).

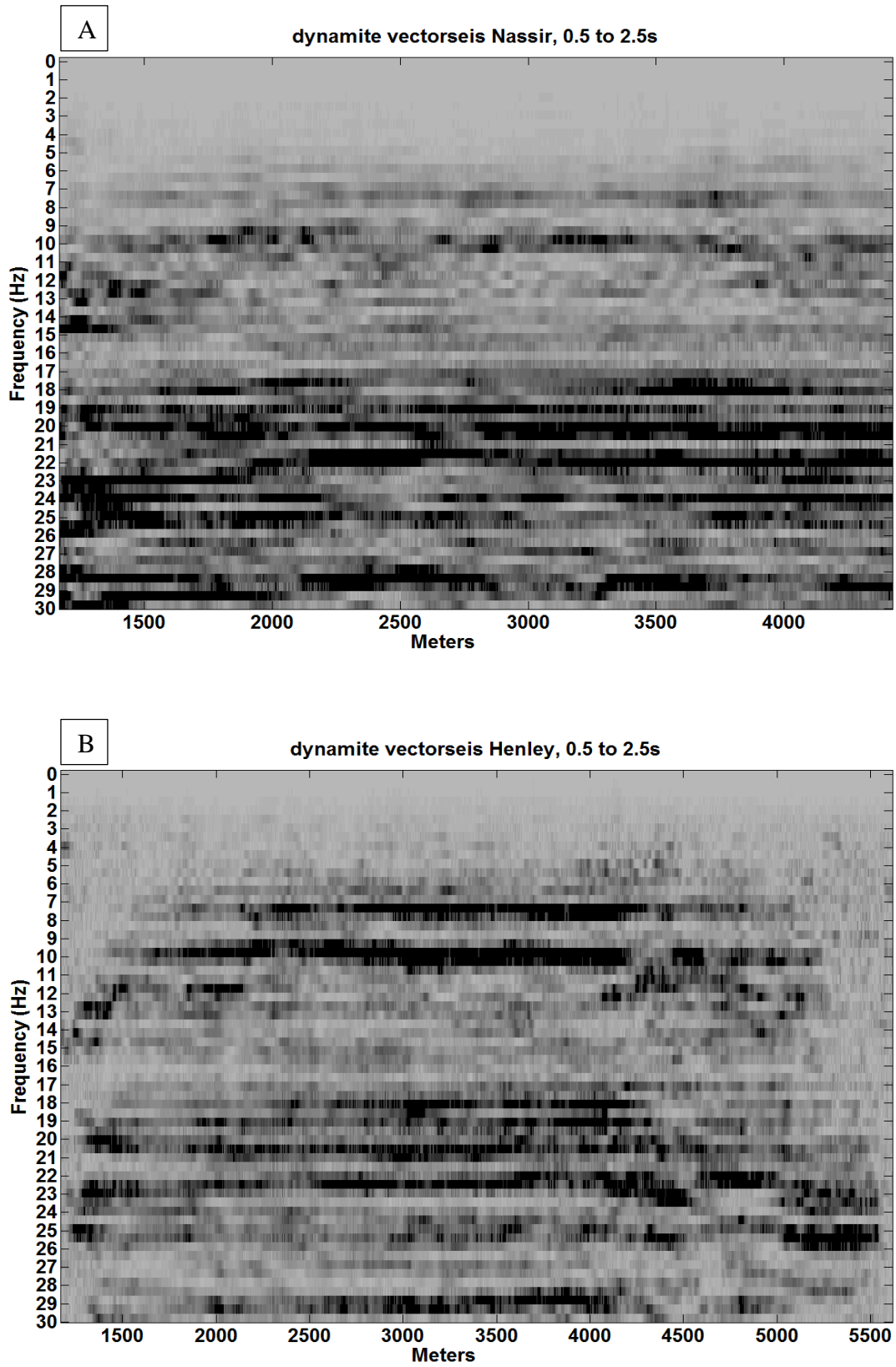


FIG.17. (A): Amplitude coherency plot for stack section for the dynamite with 10Hz 3C geophone. (B): Amplitude coherency plot for stack section for the dynamite with VectorSeis accelerometer (Henley, 2012).

REFERENCES

- Bleistein, N., Cohen, J. K. , Stockwell, J.W., Mathematics of Multidimensional Seismic Imaging, Migration, and Inversion: Springer Science press.
- Henley, D. C., 1999, Coherent noise attenuation in the radial trace domain: introduction and demonstration: CREWES Research Report.
- Henley, D. C., 2012, Interference and the art of static correction: raypath interferometry at Hussar: CREWES Research Report.
- Isaac, J. H, and Margrave, G. F., 2011, Hurrah for Hussar! Comparisons of stacked data: CREWES Research Report.
- Isaac, J. H, Margrave, G. F., Deviat, M., and Nagarajappa, P., 2013, Analyses of the low frequency content of seismic data acquired during an experiment at Hussar, Alberta, Canada: CSEG GeoConvention 2013.
- Levin, S. A., 1989, Surface-consistent deconvolution: Geophysics 54, no. 9, 1123-1133.
- Margrave, G. F., 1999, Seismic signal band estimation by interpretation of f-x spectra: Geophysics, 64, 251-260.
- Margrave, G. F., Gibson, P. C., Grossman, J. P., Henley, D. C., and Lamourex, M. P., 2004, Gabor deconvolution: theory and practice: EAGE 66th conference & Exhibition.
- Margrave, G. F., L. Mewhort, T. Phillips, M. Hall, M. B. Bertram, D. C. Lawton, K. Innanen, K. W. Hall and K. Bertram, 2012, The Hussar low-frequency experiment: CSEG Recorder, Vol. 37, No. 7, 25-39.
- Margrave, G. F., Lamourex, M. P., Grossman, J. P., and Iliescu, V., 2002, Gabor deconvolution of seismic data for source waveform and Q correction: 72nd Ann. Internat. Mtg., Soc. Expl. Geophys., Expanded Abstracts, 2190-2193.
- Saeed, A. N., 2013, Time-lapse AVO inversion: M.Sc. thesis, Univ. of Calgary.